PHYSICAL REVIEW B, VOLUME 63, 121309(R)

Optical excitations of a self-assembled artificial ion

F. Findeis, M. Baier, A. Zrenner, M. Bichler, and G. Abstreiter
Walter Schottky Institut, Technische Universität München Am Coulombwall, 85748 Garching, Germany

U. Hohenester and E. Molinari
Istituto Nazionale per la Fisica della Materia (INFM) and Dipartimento di Fisica, Università di Modena e Reggio Emilia, Via Campi 213/A, 41100 Modena, Italy

(Received 8 September 2000; published 7 March 2001)

By use of magnetophotoluminescence spectroscopy, we demonstrate bias-controlled single-electron charging of a single quantum dot. Neutral, single, and double charged excitons are identified in the optical spectra. At high magnetic fields one Zeeman component of the single charged exciton is found to be quenched, which is attributed to the competing effects of tunneling and spin-flip processes. Our experimental data are in good agreement with theoretical model calculations for situations where the spatial extent of the hole wave functions is smaller as compared to the electron wave functions.

DOI: 10.1103/PhysRevB.63.121309 PACS number(s): 78.55.Cr, 71.35.Ji, 73.21.−b, 78.66.Fd

Semiconductor quantum dots (QD's) are often referred to as artificial atoms. Different levels of neutral occupancies in QD's have been obtained in the last years by power dependent optical excitation. The associated few-particle states were intensively studied by multiexciton photoluminescence (PL) spectroscopy and corresponding theoretical investigations.[1–7] Occupancies with different numbers of electrons and holes result in charged exciton complexes. In analogy to QD's with neutral occupancy—artificial atoms—charged exciton complexes may be considered as artificial ions. In the field of low-dimensional semiconductors charged excitons were first observed in quantum-well structures.[8] In QD's, charged excitons were studied in inhomogeneously broadened ensembles by PL (Ref. 9) as well as in interband transmission experiments,[10] and recently also in single, optically tunable QD's,[11] as well as in electrically tunable quantum rings by PL.[12]

Few-particle theory predicts binding energies for charged QD excitons on the order of some meV.[11,13] This allows for the controlled manipulation of energetically well-separated few-particle states under the action of an external gate electrode. Discrete and stable numbers of extra charges are thereby possible via the Coulomb blockade mechanism. In future experiments and possible applications, the resonant optical absorption and emission of such systems is expected to be tunable between discrete and characteristic energies. Moreover such few-particle systems are expected to exhibit an interesting variety of spin configurations, which can be controlled by an external magnetic field, gate-induced occupancy, and spin-selective optical excitation. In the present paper we present, for the first time to our knowledge, experimental and theoretical results on the gate-controlled charging of a single $In_xGa_{1-x}As$ QD with an increasing number of electrons probed by magneto-PL.

For controlled charging of individual QD's a special electric-field tunable *n-i* structure has been grown by molecular-beam epitaxy. $In_{0.5}Ga_{0.5}As$ QD's are embedded in an *i*-GaAs region 40 nm above an *n*-doped GaAs layer (5×10^{18} cm^{-3}) which acts as a back contact. The growth of the QD's is followed by 270-nm *i*-GaAs, a 40-nm-thick $Al_{0.3}Ga_{0.7}As$ blocking layer, and a 10-nm *i*-GaAs cap layer. As a Schottky gate we use a 5-nm-thick semitransparent Ti layer. The samples were processed as photodiodes combined with electron-beam-structured shadow masks with apertures ranging from 200 to 800 nm. Schematic overviews of the sample and the band diagram are shown in Figs. 1(a) and 1(b). The occupation of the QD with electrons can be controlled by an external bias voltage V_B on the Schottky gate with respect to the back contact. For increasing V_B the band flattens, and the electron levels of the QD are shifted below the Fermi energy of the *n*-GaAs back contact, which results in successive single-electron charging of the QD. In our experiments excitons are generated optically at low rate and form charged excitons together with the V_B induced extra electrons in the QD. We used a HeNe laser (632.8 nm) for

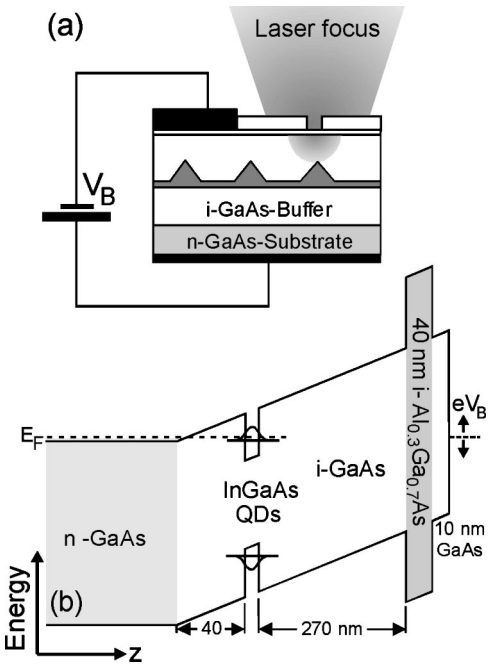

FIG. 1. (a) Photodiode combined with a near-field shadow mask. (b) Schematic band diagram of the structure for zero bias.

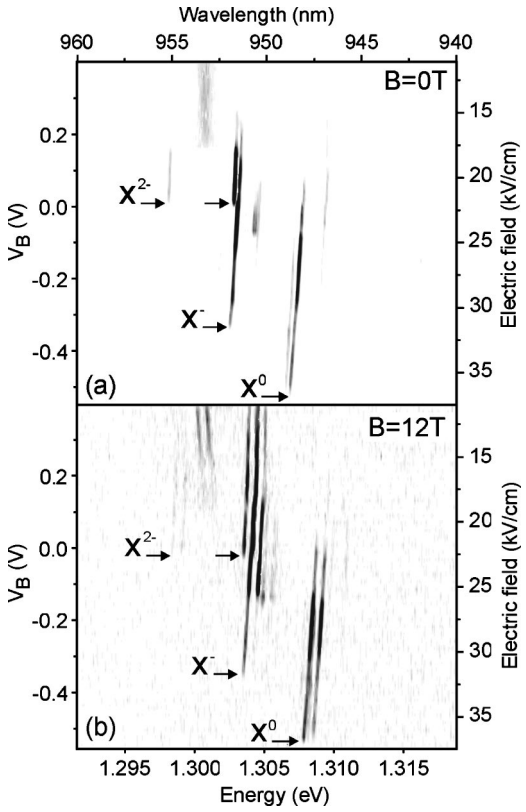

FIG. 2. Gray scale plot of the PL intensity as a function of the PL energy and V_B. The series of lines can be assigned to emissions from s-shell transitions of X^0, X^-, and X^{2-}. At zero magnetic field (a), and at $B=12$ T (b).

optical excitation, and a cooled CCD camera for detection of the PL. The sample was mounted in a confocal low-temperature, high-magnetic-field microscope.[14]

In Figs. 2(a) and 2(b) we present PL spectra as a function of V_B in the range of -550 mV to $+400$ mV, corresponding to electric fields of 37.5 to 11.1 kV/cm. The PL intensity is displayed as a gray scale plot for B=0 T in Fig. 2(a), and for $B=12$ T in Fig. 2(b). As a function of V_B we find a series of lines with discrete jumps in the emission energy. Those lines are assigned to radiative *s*-shell transitions of neutral (X^0), single charged (X^-), and double charged (X^{2-}) excitons, as marked in Figs. 2(a) and 2(b) and discussed in the following. For $B=0$ T [Fig. 2(a)] and large negative V_B ($V_B<-0.5$ V) the electron levels in the QD are far above the Fermi energy of the *n*-GaAs back contact, and the QD is electrically neutral. Optically generated excitons can relax into the QD, but before radiative recombination ($\tau\sim 1$ ns) the carriers tunnel out of the QD due to the high applied electric field. For $V_B \simeq -0.5$ V the QD is still uncharged, but in the smaller electric field radiative recombination becomes more likely and the X^0 emission line appears at 1307 meV. The weak satellite about 0.4 meV below is tentatively explained in terms of QD asymmetry.[15] With increasing V_B, the X^0 line shifts to higher energies due to the quantum-confined Stark effect in the decreasing electric field. For $V_B=-0.35$ V an emission line appears below the X^0 line at 1302.5 meV, indicating the static occupation of the QD with one electron. The X^- binding energy with respect to X^0 is determined to $\Delta E_{X^-}=4.6$ meV by the measured difference in emission energies. For -0.35 V$<V_B<0$ V the X^0 and X^- line coexist, which is a consequence of the statistical nature of nonresonant optical excitation. In the presence of one extra electron, the capture and subsequent decay of an electron-hole pair leads to the emission of a X^- photon. If only a single hole is captured we expect a X^0 photon, and if a single electron is captured we expect no photon, but instead electron back transfer to the n^+ region. At $V_B=0$ V the QD is charged with a second electron. This leads to the appearance of two characteristic emission lines [marked in Figs. 2(a) and 2(b)], which are assigned to the X^{2-} decay. The main line of the X^{2-} emission appears only 0.3 meV below the X^- line, whereas a much weaker satellite peak appears 4.6 meV below the main line at 1298.1 meV. The appearance of two emission lines is characteristic of the X^{2-} decay. The energy difference between the two X^{2-} lines corresponds to the difference in the *s*-*p* exchange energies between the two possible final states with parallel or antiparallel spin orientations of the two remaining electrons.[4] Again X^{2-} and X^- can be observed simultaneously over a certain range in V_B. At $V_B>0.19$ V only one broad emission line remains. This indicates filling of the wetting layer (WL) states with electrons. Here weakly confined electrons are interacting with the carriers in the QD, causing a broadening of the detected *s*-shell decay in the QD. A rough estimation of the V_B increment needed to bring the WL states below the Fermi energy (starting from the onset of the X^- line), taking charging energy and the electrostatics of the structure into account,[16] results in a reasonable value of $\Delta V_B=530$ mV, in good agreement with our experimental data.

For a quantitative analysis of the experimental results, we performed theoretical model calculations. Following the approach presented in Ref. 17, we assume, for electrons and holes, respectively, a confinement potential which is parabolic in the (x,y) plane and boxlike along z; despite its simplicity, such confinement is known to mimic the most important characteristics of $In_xGa_{1-x}As$ dots, and has recently proven successful in comparison with experiment.[7,18] We take 5 nm for the well width in the z direction and $\hbar\omega_0^e=30$ meV ($\hbar\omega_0^h=15$ meV) for the electron (hole) confinement energies due to the in-plane parabolic potential; material parameters are computed according to Refs. 19 and 20 (note that with these values we also well reproduce the $\sim$40-meV splitting between the $1s$ and $1p$ shells measured at higher photoexcitation powers). Finally, because of the strong quantum confinement in the z direction we safely neglect minor effects due to the applied external electric field. PL spectra for X^0, X^-, and X^{2-} are computed within a direct-diagonalization approach, accounting for all possible *e*-*e* and *e*-*h* Coulomb interactions.[11,21]

The black lines in Fig. 3 show the dependence of the luminescence spectra of the X^0, X^-, and X^{2-} lines as function of the extension L_0^h of the hole wave function (for the definition, see the figure caption). In accordance with experiment and related work,[11,12] in the PL spectra we find (for $L_0^h \leqslant L_0^e$) a redshift of the charged-exciton emission peak X^-,

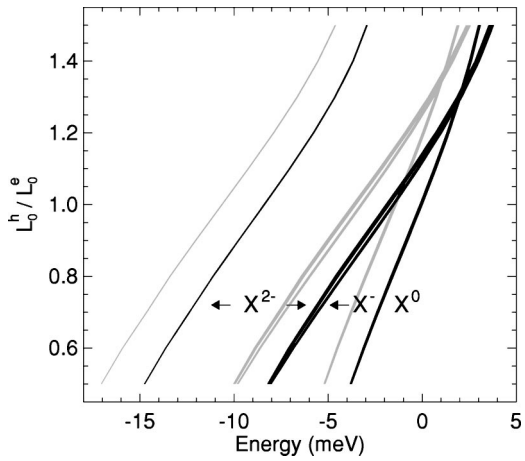

FIG. 3. Dependence of luminescence spectra on the extension of the hole wave function. $L_0^i = 1/\sqrt{(m_i \omega_0^i}$ $(i=e,h)$ is a characteristic length scale of the parabolic confinement, with m_e (m_h) the electron (hole) mass and $\hbar\omega_0^e$ $(\hbar\omega_0^h)$ the confinement energies due to the in-plane parabolic potential. Black lines: $\hbar\omega_0^e = 30$ meV ($L_0^e = 7.5$ nm) and $\hbar\omega_0^h = 15$ meV; the thickness of each line corresponds to the oscillator strength of the corresponding transition (photon energy 0 given by the X^0 energy for same extension of electron and hole wave functions, i.e., $L_0^h = L_0^e$). Gray lines: $\hbar\omega_0^e = 35$ meV ($L_0^e = 7$ nm) and $\hbar\omega_0^h = 10$ meV.

and a further, much smaller, redshift of the main X^{2-} emission peak, which is accompanied by a weak satellite peak at even lower photon energy (see arrows). A quantitative comparison between theory and experiment, however, reveals that for the same extension of electron and hole wave functions ($L_0^e = L_0^h$) the calculated charged-exciton binding of 1.5 meV is smaller by a factor of ~ 3 than the measured value; we checked that this finding does not depend decisively on small modifications of the chosen dot and material parameters. As can be inferred from Fig. 3, the X^- binding energy is a quite sensitive measure of the relative extension of electron and hole wave functions: Decreasing L_0^h and keeping all other parameters (ω_0^e, ω_0^h, L_0^e) fixed, in Fig. 3 one clearly observes an increased binding (moderate parameter changes turn out to have no impact on this general trend; see, e.g., gray lines).

We thus conclude that the large experimental X^- binding energy of 4.6 meV can only be explained by more localized hole wave functions, which we attribute to effects of heavier hole masses and possible piezoelectric fields. Additional evidence for this interpretation comes from the ratio between the exchange splitting of the two X^{2-} lines and the X^- binding energy. The experimentally observed exchange splitting of about 4.6 meV between the weak low-energy and intense high-energy branches of the X^{2-} line is found to be approximately equal to the X^- binding energy. From our theoretical investigations, such a scenario can only be obtained if the hole confinement is considerably stronger than the electron confinement.

Finally we discuss the magnetic field dependence shown in Fig. 2(b) for $B = 12$ T. From comparison with the $B = 0$ T data [Fig. 2(a)], it is clear that single-electron charging versus V_B is mostly unaffected by magnetic field. The centers of

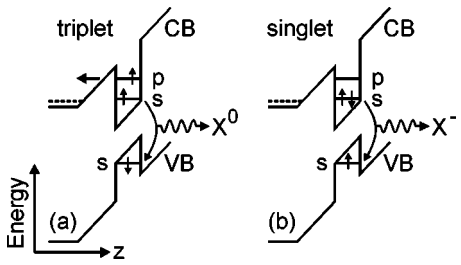

FIG. 4. Triplet (a) and singlet (b) electron configurations for X^-. The triplet state is subjected to tunnel decay from the *p* shell.

s-shell emission for X^0, X^-, and X^{2-} are shifted to higher energies due to the diamagnetic shift, and each emission line splits into two lines, separated by the Zeeman energy. The observed weak differences between the Zeeman energies of the X^0 and X^- lines seem to indicate that the spin orientation of an extra electron in the QD does not change during radiative decay from the s-shell.

In the following we concentrate on the asymmetry in the PL intensities of the two Zeeman branches of the X^- line for $-0.35\ \text{V} < V_B < -0.13$ V [see Fig. 2(b)]. This asymmetry is observed only for the X^- line, not for the X^0 and X^{2-} lines. The explanation of this phenomenon involves spin polarization, Pauli blocking, and state-selective tunneling, as summarized in Figs. 4(a) and 4(b). At $B = 12$ T a single electron in a QD is spin polarized in thermal equilibrium. The optical excitation of excitons can occur with two different spin orientations, which results in the states shown in Figs. 4(a) and 4(b). Due to Pauli blocking in the conduction band, parallel electron spin orientation leads to a metastable triplet state with one electron in the *s* shell and one in the *p* shell [see Fig. 4(a)]. If the tunneling time from the *p* shell to the continuum is shorter than the electron spin-flip time, an electron is lost, and we end up with a neutral exciton and hence with a contribution to one Zeeman component of the X^0 line, i.e., we lose one Zeeman component of the X^- decay. The introduction of an exciton with opposite spin orientation, however, produces a singlet state as shown in Fig. 4(b). The radiative decay of this configuration contributes to the other Zeeman component of the X^- line. Our findings also imply that the associated heavy-hole spin-flip time should be at least of the same order or longer than the *e-h* lifetime. Long spin-flip times and conservation of the exciton spin within the exciton lifetime were already reported for zero-dimensional systems at high magnetic fields.[22] The suppression of one X^- Zeeman component persists over a V_B range of 0.22 V, which translates to an energy shift of the QD states with respect to the n-GaAs Fermi energy of 28 meV (approximately to the conduction-band *s-p* separation). For $V_B > -0.13$ V both Zeeman components of the X^- line are recovered as a consequence of the increased tunneling time, which now allows for the competing spin-flip and relaxation process to the *s* shell. For the X^0 and X^{2-} lines, a quenching of Zeeman lines is not expected and also not observed, since the *p* shell is either never (X^0) or always (X^{2-}) populated, regardless of the spin orientation of the optically excited *e-h* pair.

In summary, we have demonstrated bias-controlled charg-

ing of a single QD in magneto-optic PL experiments. The few-particle interaction energies determined experimentally for the X^- and X^{2-} states are found to be in good agreement with our theoretical model for situations where the spatial extent of the hole wave functions is smaller as compared to the electron wave functions. Spin polarization and lifting of the Zeeman degeneracy at high magnetic fields allows further access to the so-far-unexplored spin-dependent properties of few-particle states. The suppression of one Zeeman component of the X^- decay is explained in terms of state-selective tunneling from a spin-triplet configuration.

This work was supported financially by the DFG via SFB 348, by the BMBF via 01BM917, in part by INFM through PRA-99-SSQI, and by the EU under the TMR Network ''Ultrafast Quantum Optoelectronics'' and the IST programme ''SQID.''

[1] For a recent review, see A. Zrenner, J. Chem. Phys. **112**, 7790 (2000).
[2] E. Deckel *et al.*, Phys. Rev. Lett. **80**, 4991 (1998).
[3] L. Landin *et al.*, Science **280**, 262 (1998).
[4] P. Hawrylak, Phys. Rev. B **60**, 5597 (1999).
[5] U. Hohenester, F. Rossi, and E. Molinari, Solid State Commun. **111**, 187 (1999).
[6] F. Findeis, A. Zrenner, G. Böhm, and G. Abstreiter, Solid State Commun. **114**, 227 (2000).
[7] M. Bayer *et al.*, Nature (London) **405**, 923 (2000).
[8] K. Kheng *et al.*, Phys. Rev. Lett. **71**, 1752 (1993).
[9] K. H. Schmidt, G. Medeiros-Ribeiro, and P. M. Petroff, Phys. Rev. B **58**, 3597 (1998).
[10] R. J. Warburton *et al.*, Phys. Rev. Lett. **79**, 5282 (1997).
[11] A. Hartmann *et al.*, Phys. Rev. Lett. **84**, 5648 (2000).
[12] R. J. Warburton *et al.*, Nature (London) **405**, 926 (2000).
[13] A. Wojs and P. Hawrylak, Phys. Rev. B **55**, 13 066 (1997).
[14] A. Zrenner *et al.*, Physica B **256-258**, 300 (1998).
[15] D. Gammon *et al.*, Phys. Rev. Lett. **76**, 3005 (1996).
[16] H. Drexler *et al.*, Phys. Rev. Lett. **73**, 2252 (1994).
[17] G. A. Navarez and P. Harylak, Phys. Rev. B **61**, 15 753 (2000).
[18] P. Hawrylak, G. A. Navarez, M. Bayer, and A. Forchel, Phys. Rev. Lett. **85**, 389 (2000).
[19] O. Stier, M. Grundmann, and D. Bimberg, Phys. Rev. B **59**, 5688 (1999).
[20] We use $m_z^h = 1/(\gamma_1 - 2\gamma_2)$ and $m_\parallel^h = 1/(\gamma_1 + \gamma_2)$ for the hole mass in the z and lateral directions, with γ_i the Luttinger parameters.
[21] For details of our computational approach, see U. Hohenester and E. Molinari, Phys. Status Solidi B **221**, 19 (2000). In our calculations we consider a single-particle basis of the six electron and hole states with lowest energies, respectively.
[22] W. Heller and U. Bockelmann, Phys. Rev. B **55**, R4871 (2000).